Reynolds number effects on scale energy balance in wall turbulence

Neelakantan Saikrishnan, Elisabetta De Angelis, Ellen K. Longmire, Ivan Marusic, Carlo M. Casciola et al.

Citation: Phys. Fluids **24**, 015101 (2012); doi: 10.1063/1.3673609
View online: http://dx.doi.org/10.1063/1.3673609
View Table of Contents: http://pof.aip.org/resource/1/PHFLE6/v24/i1
Published by the American Institute of Physics.

Reynolds number effects on scale energy balance in wall turbulence

Neelakantan Saikrishnan,[1,a)] Elisabetta De Angelis,[2] Ellen K. Longmire,[3] Ivan Marusic,[4] Carlo M. Casciola,[5] and Renzo Piva[5]
[1]*Department of Biomedical Engineering, Georgia Institute of Technology, 315 Ferst Drive NW, Room 2116, Atlanta, Georgia 30332, USA*
[2]*DIEM, Università di Bologna, Via Fontanelle 40, 47121 Forlì, Italy*
[3]*Department of Aerospace Engineering and Mechanics, University of Minnesota Twin Cities, 110 Union Street SE, 117B Akerman Hall, Minneapolis, Minnesota 55455, USA*
[4]*Walter Bassett Aerodynamics Laboratory, Department of Mechanical Engineering, University of Melbourne, Victoria 3010, Australia*
[5]*Dipartimento di Meccanica e Aerospaziale, Sapienza Università di Roma, Via Eudossiana 18, 00184 Roma, Italy*

(Received 10 August 2011; accepted 24 November 2011; published online 17 January 2012)

The scale energy budget utilizes a modified version of the classical Kolmogorov equation of wall turbulence to develop an evolution equation for the second order structure function [R. J. Hill, "Exact second-order structure-function relationships," J. Fluid Mech. **468**, 317 (2002)]. This methodology allows for the simultaneous characterization of the energy cascade and spatial fluxes in turbulent shear flows across the entire physical domain as well as the range of scales. The present study utilizes this methodology to characterize the effects of Reynolds number on the balance of energy fluxes in turbulent channel flows. Direct numerical simulation data in the range $Re_\tau = 300$–934 are compared to previously published results at $Re_\tau = 180$ [N. Marati, C. M. Casciola, and R. Piva, "Energy cascade and spatial fluxes in wall turbulence," J. Fluid Mech. **521**, 191 (2004)]. The present results show no Reynolds number effects in the terms of the scale energy budget in either the viscous sublayer or buffer regions of the channel. In the logarithmic layer, the transfer of energy across scales clearly varies with Reynolds number, while the production of turbulent kinetic energy is not dependent on Reynolds number. An envelope of inverse energy cascade is quantified in the buffer region within which energy is transferred from small to larger scales. This envelope is observed in the range $6 < y^+ < 37$, where all scales except the smallest scales display characteristics of an inverse energy cascade. The cross-over scale l_c^+, which indicates the transition between production dominated and scale transfer dominated regimes, increases with Reynolds number, implying a larger range of transfer dominated scales, before the dominant mechanism switches to production. At higher Reynolds numbers, two distinct regimes of l_c^+ as a function of wall-normal location are observed, which was not captured at $Re_\tau = 180$. The variations of l_c^+ match the trends of the shear scale, which is a representation of the mean shear in the flow. Thus, this study demonstrates the utility and importance of the use of higher Reynolds number data in order to accurately characterize and understand the energy dynamics of various scales across the entire boundary layer. © *2012 American Institute of Physics*. [doi:10.1063/1.3673609]

I. INTRODUCTION

Wall-bounded turbulent flows such as boundary layers, pipe flows, and channel flows are characterized by a mean velocity gradient, which produces a strong inhomogeneity in the energy flux in the wall-normal direction. This leads to the traditional classification of the momentum

[a)]Electronic mail: neela.saikrishnan@gatech.edu.

deficit region based on the mean velocity profile into four generic layers: the viscous sublayer, the buffer layer, the logarithmic layer, and the outer flow. Recent studies have also discussed an alternate four layer description of wall-bounded turbulent flows based on the mean momentum balance equation for turbulent flows,[3,4] where each layer is characterized by varying interplay of the pressure gradient term, the gradient of the viscous stresses and the gradient of the Reynolds stresses. In both of these definitions, the energy fluxes between the regions drive the local energetics in each region (the "physical space" approach). Simultaneously, at a given wall-normal location, the interaction between eddies of different sizes is typically characterized by the energy cascade, such that the flow field is decomposed into a hierarchy of eddy scales. Turbulent kinetic energy (TKE) is produced at the largest scales by the action of shear, transferred to smaller eddies, and dissipated at the smallest scales by viscosity. This spectral or "scale space" approach enables an understanding of the distribution and flux of energy across various length scales of eddies. A combination of both approaches is necessary to understand how the energy associated with a specific scale of motion is transferred both to other length scales and across regions of shear.

The classical Kolmogorov equation based on the second order structure function $\langle \delta u^2 \rangle$ or scale-energy provides a good starting point for developing a methodology combining the "physical space" and "scale space" approaches. A generalized form of this equation for inhomogeneous conditions such as shear flows has been developed previously to simultaneously characterize TKE dynamics across a range of scales and wall-normal locations.[1] This equation was used by Marati *et al*. to analyze direct numerical simulation (DNS) data of a turbulent channel flow at $Re_\tau = 180$ ($Re_\tau = \delta U_\tau/\nu$, where δ is the channel half-height and U_τ is the friction velocity).[2] In that study, it was demonstrated that the conventional definition of the channel in terms of viscous layer, buffer region, log-layer, and outer region was applicable even in the context of the scale energy balance. The production of scale energy was predominant in the buffer region, while the log layer has a constant flux of energy into the bulk of the flow. In scale space, production of scale energy was dominant in the largest scales, followed by a range of predominant transfer, down to the smallest scales where diffusion and dissipation dominate. Additionally, this study suggested the presence of an inverse cascade of energy from the small to the larger scales in the viscous sublayer.

The effects of Reynolds number on turbulent stresses and TKE have been a subject of inquiry in a number of studies[5–9] and have recently been studied over a range of Reynolds numbers, $Re_\tau = 186$, 587, 934, and 2003.[10] The primary quantities of interest in these studies were the TKE production and dissipation. The magnitude of production increased with Reynolds number in the buffer region, whereas the dissipation calculated using the assumption of isotropy increased with Reynolds number in the viscous sublayer. The increase in dissipation could be due to the presence of large scale "inactive motions."[11] In the logarithmic and outer regions, no significant Reynolds number variations were observed in the production or dissipation. The ratio of the production to the dissipation is a measure of the equilibrium nature of the logarithmic region, and characteristics of an equilibrium layer start to appear for $Re_\tau = 590$ and above. The peak value of production, seen in the buffer region, increased with Reynolds number.

Given the Reynolds number effects observed for single point statistics, the aim of the present work is to extend the scale energy analysis conducted by Marati *et al*. at $Re_\tau = 180$ to higher Reynolds numbers.[2] Thus, the scale energy dynamics are examined using DNS data of turbulent channel flows at $Re_\tau = 298$, 587, and 934 in this study. Details of the DNS datasets and the processing methodology are presented in Sec. II. The variations of scale energy and the scale energy budget at specific locations in the boundary layer are presented and discussed in Sec. III, and some conclusions from this study are provided in Sec. IV.

II. METHODOLOGY

A. Description of DNS datasets

All results in this paper are based on four DNS datasets of turbulent channel flows in the Reynolds number range $Re_\tau = 180$–934. The references to the sources of these data and relevant parameters are indicated in Table I. All quantities are normalized using inner variables. The streamwise, wall-normal, and spanwise directions are along the x, y, and z axes, respectively, and the velocity components along these three directions are represented as U, V, and W. Capital

TABLE I. Parameters of the DNS datasets. Details of the datasets are available in **Re180**;[2] **Re300**;[13] **Re590**;[8] **Re934**.[14] The wall-normal spacings Δy^+ indicated are at the center of the channel.

Dataset	Re_τ	L_x/δ	L_z/δ	$N_x \times N_y \times N_z$	Δx^+	Δy^+_{max}	Δz^+
Re180	178	4	2	$256 \times 129 \times 128$	2.8	4.4	2.8
Re300	298	2π	π	$512 \times 193 \times 256$	3.7	4.9	3.7
Re590	587	2π	π	$384 \times 257 \times 384$	9.6	7.2	4.8
Re934	934	8π	3π	$2048 \times 385 \times 1536$	11.5	7.6	5.7

letters refer to mean quantities and lower-case ones to fluctuating quantities. The brackets represent ensemble averaging over homogeneous directions, usually over wall-parallel planes and time. The first two datasets were characterized by small domains with high spatial resolution, while the latter two datasets were characterized by much larger domains and a somewhat coarser resolution. All the datasets were obtained using numerical codes that integrated the Navier-Stokes equations in the form of evolution problems for the wall-normal vorticity and the Laplacian of the wall-normal velocity.[12] The spatial discretization used de-aliased Fourier expansions in wall-parallel planes and Chebyshev polynomials in the wall-normal direction.

B. Two point scale energy budget

The second-order structure function $\langle \delta u^2 \rangle$, where $\delta u^2 = \delta u_i \delta u_i$, $\delta u_i = u_i(x_s + r_s) - u_i(x_s)$ is the fluctuating velocity increment and $\langle\rangle$ represents ensemble averaging, can be interpreted as the amount of energy associated with a given scale $r = \sqrt{r_s r_s}$.[15] This quantity is a function of the separation vector r_i and the mid-point $X_{ci} = 0.5(x'_i + x_i)$.

For a planar channel or pipe flow, a simultaneous view of spatial fluxes and scale processes can be achieved by a suitable generalization of the scale energy budget as,

$$\nabla_r \cdot \langle \delta u^2 \delta \mathbf{u} \rangle + \left(2\langle \delta u \delta v \rangle \left(\frac{dU}{dY_c} \right)^* + \frac{\partial \langle v^* \delta u^2 \rangle}{\partial Y_c} + 2\frac{\partial \langle \delta p \delta v \rangle}{\rho \partial Y_c} \right) = 2\nu \left(\nabla_r^2 + \frac{\partial^2}{8\partial Y_c^2} \right) \langle \delta u^2 \rangle - 4\epsilon^*, \quad (1)$$

where the asterisk defines a mid point average, e.g., $\epsilon^* = (\epsilon(x_i) + \epsilon(x'_i))/2$.[1] Terms with r-derivatives are related to the flux through scales while those with Y_c-derivatives arise due to physical inhomogeneity. Equation (1) holds when the two points considered lie at the same wall-normal location, see also Marati *et al*. for a more detailed derivation.[2]

In order to evaluate an effective contribution at given values of r and Y_c for all the terms in Eq. (1), we introduce an r-average and the r-averaged form of Eq. (1) is given by

$$T_r(r, Y_c) + \Pi(r, Y_c) + T_c(r, Y_c) + P(r, Y_c) = D_r(r, Y_c) + D_c(r, Y_c) + E(r, Y_c). \quad (2)$$

Here, T_r is the inertial flux through the scales, Π accounts for production, T_c is the inertial contribution to the buildup of the spatial flux of scale energy and is strictly associated with inhomogeneity, and P is an inhomogeneous contribution related to the pressure-velocity correlation. On the right hand side, E is the dissipation term, while D_r and D_c are the diffusive contributions to the flux through the scales and the spatial flux, respectively. The terms of Eq. (2) can be combined and recast as

$$T_r(r, Y_c) + \Pi_e(r, Y_c) = D_e(r, Y_c) + E(r, Y_c) = E_e(r, Y_c), \quad (3)$$

where Π_e is the effective production accounting for production, physical space transfer, and the pressure-velocity correlation, D_e is the effective diffusion accounting for physical space diffusion and scale space diffusion, while E_e is the effective dissipation consisting of the effective diffusion and the dissipation. This can be interpreted that the sum of transfer through the scales (T_r) and effective production (Π_e) is balanced by the dissipative and diffusive contributions (E_e). Moreover, an inspection of the individual terms of Eq. (3) in the $r - Y_c$-plane can be very useful, since this provides a direct method of determining the relative dominance of terms at every wall-normal location and scale.

III. RESULTS AND DISCUSSION

A. Single point statistics of DNS datasets

The mean velocity and turbulence intensity profiles for all these datasets are available in the references listed in Table I. The variation of the mean velocity and turbulence intensity profiles with Reynolds number are identical to the trends observed in Hoyas *et al.*[10] For all datasets, the peak of the streamwise turbulent intensity u^+_{rms} is located at $y^+ = 16$. The profile of v^+_{rms} has the smallest magnitude among the three velocity components, and this quantity increases with y^+ until $y^+ \sim 50$, beyond which it decreases very slowly. Similarly, the profile of w^+_{rms} increases with y^+ until $y^+ \sim 50$, and decreases very gradually for larger y^+. The magnitudes of u^+_{rms} match in the range $y^+ < 16$ for all Reynolds numbers, beyond which the magnitude is larger for the higher Reynolds numbers. The magnitudes of v^+_{rms} and w^+_{rms} increase with Reynolds number for all y^+, with an increasing difference as y^+ increases.

The trends of the single point turbulence kinetic energy balance also match the findings in Hoyas *et al.*[10] The peak of production occurs in the buffer region at $y^+ = 12$–16. A significant amount of this energy is dissipated locally, while the excess feeds turbulent convection and diffusion. The equilibrium nature of the logarithmic region is observed in spite of the moderate Reynolds numbers used here. This trend continues through the outer logarithmic layer, where the magnitudes of all the terms reduce to near zero. The production and dissipation increase with increasing Reynolds number, whereas the convective and diffusive terms remain relatively constant. The peak value of production increases with Reynolds number in this range and asymptotes towards the limit for infinite Reynolds numbers equal to 0.25.[16] These observations regarding the production and dissipation are consistent with similar results presented by Abe *et al.*, Fisher *et al.*, Moser *et al.*, and Hoyas *et al.*[8–10,17]

B. Variation of scale energy with Reynolds number

Figure 1(a) shows the variation of the scale energy as a function of the wall-normal location y^+ and the streamwise scale r^+_x, while Figure 1(b) shows the scale energy as a function of y^+ and spanwise scale r^+_z for **Re590** and **Re934**. For the corresponding plots from **Re180**, see Marati *et al.*[2] These figures focus on the variation of scale energy in the small length scales, up to 250 viscous units.

In order to analyze the behavior of $\langle \delta u^2 \rangle$ for finite values of the scales and distance from the wall, the plane $(r^+_{x/z}, y^+)$ is divided into two areas by a straight line representing κy^+. In the logarithmic region of the boundary layer, the shear scale $L_s = \sqrt{\langle \epsilon \rangle / S^3}$, where $S = dU/dy$. Recently, the scaling of mixed structure functions in turbulent boundary layers based on experimental data from

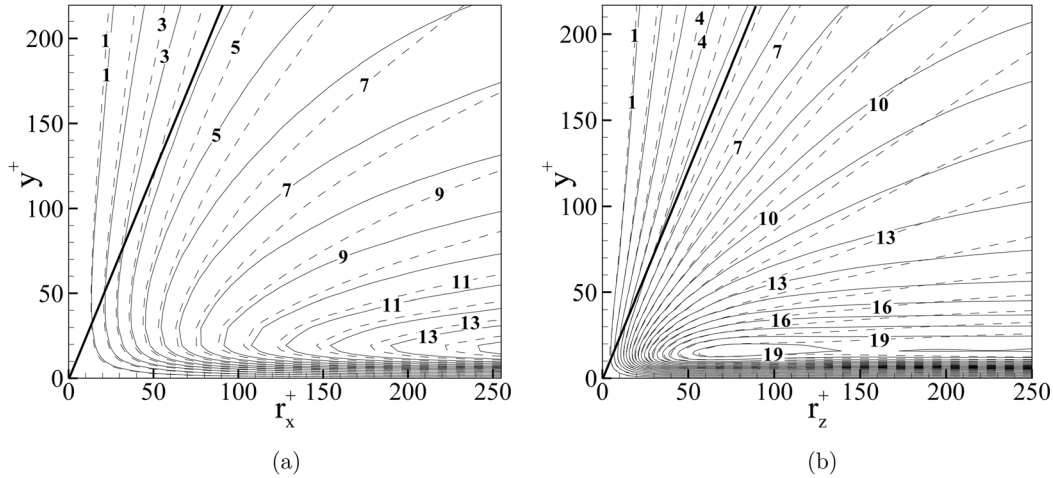

FIG. 1. (a) Isolines of $\langle \delta u^2(r^+_x, 0, 0|y^+) \rangle$ in the (r^+_x, y^+) plane. (b) Isolines of $\langle \delta u^2(0, 0, r^+_z|y^+) \rangle$ in the (r^+_z, y^+) plane. Solid isolines are from **Re590** and dashed isolines are from **Re934**. Numbers on the isolines indicate the value of that specific isoline. The heavy solid line is κy^+.

x-wires was discussed in Jacob *et al.*[18] The authors demonstrated that the anisotropic behavior of the fluctuations throughout the boundary layer could be understood in terms of a superposition of two distinct regimes. Further, the scale at which the transition between these regimes occurs is controlled by the magnitude of the mean shear, which manifests itself in the shear scale. Below the shear scale, an isotropy-recovering behavior occurs, which is characterized by dimensional predictions based on Lumley's argument.[19] Above the shear scale, the anisotropy introduced by the flow modifies the isotropic scaling laws predicted by Lumley. Further, it was observed that the isotropic behavior is much more prominent farther away from the wall. In the area characterized by the theoretical isotropy recovery, using the Kolmogorov scaling yields $\langle \delta u^2 \rangle \propto \epsilon^{2/3} r^{2/3}$. In the logarithmic layer, if the equilibrium layer concept is used, the following expression is obtained $\langle \delta u^2 \rangle \simeq \kappa^{2/3} u_\tau^2 (r/y)^{2/3}$, and hence in the region to the left of the shear scale, the isolines of the scale energy should be straight lines fanning out of the origin. Such an expectation is reasonably confirmed in the plots in Figure 1, where the data for **Re934** show a more marked trend toward this linear behavior of the isolines than for **Re590** and the corresponding isolines for **Re180** shown in Marati *et al.*[2] Regarding the areas outside the isotropy recovery region, the effect of Reynolds number becomes more apparent, i.e., the curves for the different Reynolds numbers diverge, with a larger value of $\langle \delta u^2 \rangle$ for the larger Reynolds number at the same wall-normal location and scale.

The maximum of the scale energy occurs along the line $y^+ = 16$ for both Reynolds numbers, which is consistent with the peak of production from single point TKE statistics. The contours of the largest value of scale energy are not closed at the highest r_x^+ shown ($r_x^+ = 250$), and therefore, the maximum value of scale energy must occur at a larger scale. An analysis of variation of scale energy up to $r_x^+ \sim 1200$ was conducted for the higher Reynolds numbers, and still no peak of the scale energy in the longitudinal direction was observed. This result appears consistent with the long streamwise correlations found in turbulent boundary layers.[20] Previous studies[20–23] have documented the presence of an inner peak in spectrograms corresponding to $y^+ \approx 15$, $\lambda_x^+ \approx 1000$, where k_x and λ_x^+ are the streamwise wavenumber and wavelength, respectively, and $\lambda_x^+ = 2\pi/k_x$. The inner peak is believed to relate to the near-wall cycle and associated near-wall streaks reported in Kline *et al.*[24] The fact that we do not observe such a peak appears to highlight one difference between the current analysis conducted using the physical displacement r_x^+ and spectral analysis that determines a streamwise wavelength λ_x^+.

In comparison, the correlations in the spanwise direction are shorter. Comparing the scale energy values at the larger scales, we observe that the gradient of scale energy with y^+ is much larger in Figure 1(b) than the corresponding ones from Figure 1(a), indicated by the closely spaced contour levels in the range $y^+ < 50$. The peak of the scale energy occurs at $y^+ = 16$ and $r_z^+ = 70$ for **Re590**. The scale energy increases with y^+ in the range $10 < y^+ < 16$, while it decreases with y^+ for $y^+ > 16$. The scale energy is relatively independent of r_z^+ until $y^+ \sim 50$, and beyond this, the scale energy increases with increasing r_z^+.

At the smallest scales ($r_x^+ < 30$ in Figure 1(a), $r_z^+ < 30$ in Figure 1(b)), the scale energy which matches for both Reynolds numbers does not vary with y^+. The data from the two Reynolds numbers starts deviating at larger scales. At locations further from the wall, the scale at which $\langle \delta u^2 \rangle$ from the two Reynolds numbers diverges reduces. For example, in Figure 1(b), the scale energies of the two Reynolds numbers diverge at $r_z^+ = 65$ at $y^+ = 50$, and at $r_z^+ = 25$ at $y^+ = 100$. At larger scales, the scale energy appears independent of Reynolds number only in the viscous sublayer and buffer regions. The difference in scale energy between the two Reynolds numbers increases with increasing scale. Similarly, with increasing y^+, the difference between scale energy between the two Reynolds numbers increases. For example, consider 4 points on Figure 1(b) representing combinations of scales and wall-normal locations: $(r_z^+, y^+) = (50, 50), (50, 150), (150, 50)$ and (150,150). The differences in scale energy between the two Reynolds numbers at these points are 0, 0.25, 0.70, and 0.79, respectively. Thus, Reynolds number effects are observed with increasing scale as well as increasing wall-normal location.

C. Variation of terms of energy budget with Reynolds number

Figures 2–4 show the trends in the terms of the scale energy balance at various locations in the channel. The four locations represented in these figures are $y^+ = 10$ (lower buffer region), $y^+ = 100$,

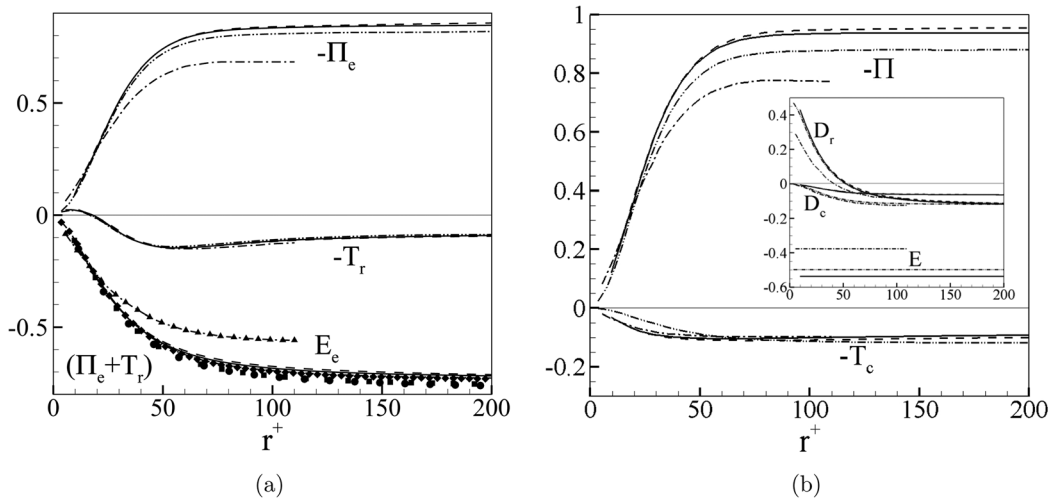

FIG. 2. (a) Scale energy balance at $y^+ = 10$ (viscous sublayer/buffer region). (b) Individual contributions of terms from (a). $-\Pi_e$ is the effective production; $-T_r$ is the transfer in scale space; E_e is the effective dissipation; filled symbols represent $(\Pi_e + T_r)$. Dashed lines and filled circles are from **Re934**; solid lines and filled squares are from **Re590**; dashed-dotted-dotted lines and filled diamonds are from **Re300**; dashed-dotted lines and filled triangles are from **Re180**. $-\Pi$ is the turbulent production; $-T_c$ is the transfer in physical space; E is the turbulent dissipation; D_r and D_c are the diffusion in r-space and physical space, respectively.

$y^+ = 250$, and $y/\delta = 0.8$ (outer region). In all these figures, the effective production (Π_e) and scale transfer (T_r) terms are indicated with a negative sign for ease of presentation. The filled symbols show the sum of Π_e and T_r, which is expected to balance the effective dissipation E_e.

For all Reynolds numbers and wall-normal locations, $-\Pi_e$ and E_e increase with increasing r^+ before reaching a constant value, while $-T_r$ increases initially with r^+ and decreases at larger scales. Looking at the individual terms in Figures 2(b) and 3(b), the production term $-\Pi$ increases in magnitude similar to $-\Pi_e$. The spatial flux of scale energy $-T_c$ is relatively small in the viscous sublayer, buffer region and logarithmic region, implying that $-\Pi$ is the major contributor to $-\Pi_e$. In the outer layer, the magnitudes of all terms are very small, and $-T_c$ becomes comparable to $-\Pi$. $-T_c$ remains almost constant for all r^+. The scale space diffusion D_r is maximum at the smallest scale and reduces to almost zero at larger scales. The physical space diffusion D_c has a small non-zero value only at $y^+ = 10$, while remaining zero at other locations. In general, E_e becomes equal to E at large scales. It must be kept in mind that all the terms shown here are

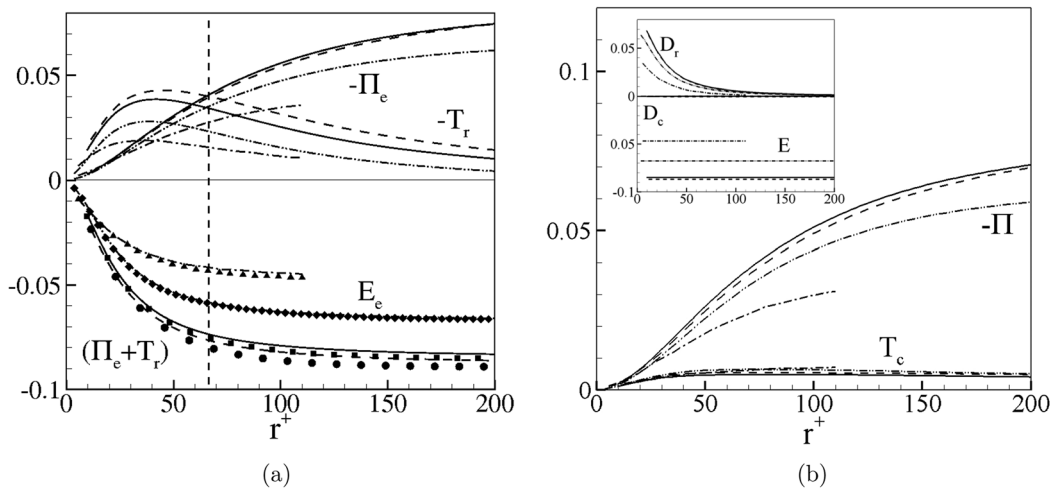

FIG. 3. (a) Scale energy balance at $y^+ = 100$ (inner logarithmic region). (b) Individual contributions of terms from (a). Definitions of the various terms are the same as in Figure 2. The vertical dashed line in (a) represents the cross-over scale at $Re_\tau = 934$.

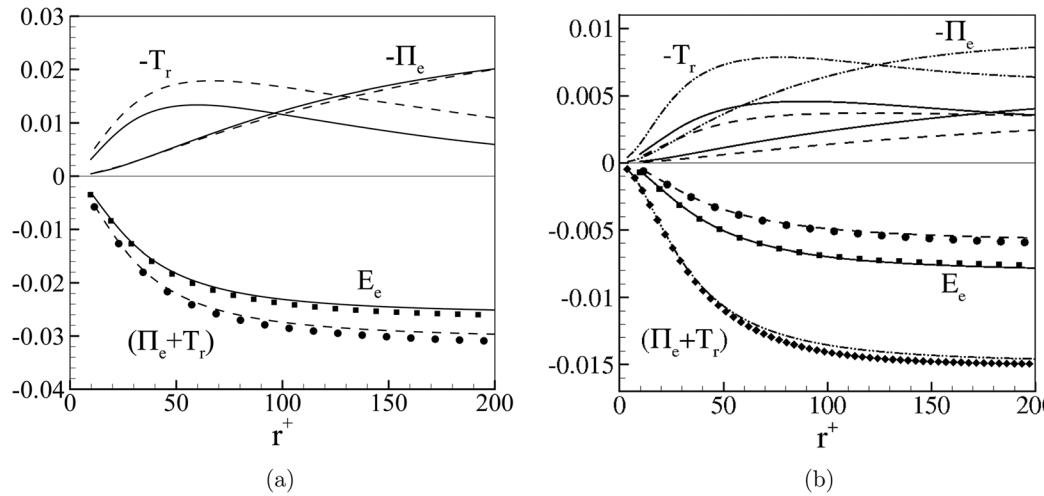

FIG. 4. (a) Scale energy balance at $y^+ = 250$ (outer logarithmic region). (b) Scale energy balance at $y/\delta = 0.8$ (outer region). Definitions of the various terms are the same as in Figure 2. Dashed lines and filled circles are from **Re934**; solid lines and filled squares are from **Re590**.

averaged in r-space. The total imbalance between the terms, indicated by the difference between the curve for E_e and the filled symbols, is very small for all Reynolds numbers. The difference between these two terms is the contribution of the pressure term, which was not evaluated in the current study.

The qualitative trends observed for the various terms at $y^+ = 10$ in Figure 2(a) do not change with Reynolds number. However, the actual magnitudes of certain terms are different for the two lower Reynolds numbers, **Re180** and **Re300**, while all the terms from **Re590** and **Re934** match almost exactly over the entire range of scales. $-\Pi_e$ is significantly lower at **Re180** than for the other three Reynolds numbers, which lie very close to one another. This suggests that the range of scales at $Re_\tau = 180$ is insufficient to capture the dynamics observed in higher Reynolds number flows. $-T_r$ matches exactly for all the datasets, which suggests that the influence of E_e is also higher at the three higher Reynolds numbers.

In comparison, the scale energy balance at $y^+ = 100$ shown in Figure 3(a) shows that $-\Pi_e$ increases with Reynolds number from **Re180** to **Re590**, while curves from **Re590** and **Re934** match each other extremely closely over the range of scales shown in this plot. A possible explanation for this might be that this location is nominally in the logarithmic layer for **Re590** and **Re934**, whereas it is in the outer layer for **Re180** and **Re300**. Further, a smaller range of eddy scales exists for **Re180** and **Re300**, and there is no distinct separation between the inner and outer layers. By contrast, $-T_r$ increases steadily from **Re180** to **Re934**, indicating a larger energy transfer with increasing Reynolds number. At r^+ up to 1200 for **Re590** and **Re934** (results not shown here), it was observed that **Re934** had a larger magnitude of both $-\Pi_e$ and $-T_r$ than **Re590**. This might be because the effect of Reynolds number on $-\Pi$ becomes more prominent with increasing scales and therefore is noticeable only at the larger scales.

Figures 2(b) and 3(b) show the individual contributions of the terms of the scale energy budget as described in Eq. (2). At $y^+ = 10$, $-T_c$ is negative for all scales at all Reynolds numbers, while it is always positive at $y^+ = 100$. Thus, the role of $-T_c$ in $-\Pi_e$ is reversed between the buffer region and the logarithmic region. While scale energy is locally removed from the viscous sublayer, it is locally added to the logarithmic region. However, smaller $-T_c$ implies that this addition of scale energy is very small. The magnitudes of the terms in the inset of both figures are different between **Re180** and the three larger Reynolds numbers. At $y^+ = 10$, D_c is largest and D_r is smallest for **Re180**. The combined effect of these two terms provides a nearly constant value of net diffusion for the three higher Reynolds numbers, suggesting that the effect of increased $-\Pi$ at larger Reynolds numbers is directly balanced only by an increased amount of E in the buffer region. At $y^+ = 100$, the negligible role of $-T_c$ and D_c suggests that this region contains dynamics similar to homogeneous shear

flow.[25] However, in the boundary layer, this region is traversed by a nearly constant flux of turbulent kinetic energy away from the wall, unlike in a homogeneous shear flow.

Further from the wall ($y^+ = 250$) shown in Figure 4(a) for **Re590** and **Re934**, the magnitudes of the terms are smaller than those at $y^+ = 100$ because the overall scale energy dynamics become weaker with increasing y^+. For **Re590**, $y^+ = 250$ equals $y/\delta = 0.43$, where the logarithmic law of the wall and inner scaling no longer apply, but the curves are presented here for completeness. At this location, curves of $-\Pi_e$ from **Re590** and **Re934** match each other very closely, with $-\Pi$ again being the dominant contributor. As at $y^+ = 100$, $-T_r$ at $y^+ = 250$ increases with increasing Reynolds number over the full range of r^+ plotted, suggesting a larger magnitude of energy being transferred between the scales at larger Reynolds numbers.

In general, the scale energy terms decrease with increasing y^+, mainly due to smaller populations of eddies and reduced interactions between them. As y^+ increases, the contribution of the mean shear becomes smaller and smaller. A conventional method of comparing quantities in the outer layer is by comparing the same wall-normal location normalized with the channel half-width, as opposed to normalizing with inner variables U_τ and ν. Figure 4(b) shows results from the scale energy budget at $y/\delta = 0.8$ at the three higher Reynolds numbers. In this region, the magnitude of each term decreases with increasing Reynolds number. For example, $-\Pi_e$ and $-T_r$ for **Re300** are almost twice as large as the same terms from **Re590**, which in turn are larger than the corresponding terms from **Re934**. This is expected since the dynamics in the outer region are weaker at larger Reynolds numbers where interactions from the opposing half of the channel play a weaker role.

D. Dynamics of transfer terms: the inverse energy cascade

To understand the dynamics of the transfer terms in the viscous sublayer and the buffer region, contour plots of these terms are presented in Figure 5. For completeness, these plots are shown up to $y^+ = 100$, which extends into the inner part of the logarithmic region. In the range of y^+ shown, the values of T_r and T_c from **Re590** and **Re934** match each other almost identically, so only results from **Re590** are presented for discussion. By definition, $T_r(r^+,y^+)$ is the transfer of turbulent kinetic energy at a given y^+ and r^+. This quantity is averaged over r-space, which implies that the value of T_r at scale r^+ includes the combined effect of all scales smaller than or equal to r^+. When T_r is negative, it implies that energy is transferred into the domain of scale r^+ from scales larger than r^+. This is the conventional cascade of energy in turbulence. When T_r is positive, a net inverse cascade occurs in which energy is transferred from the small to large scales.

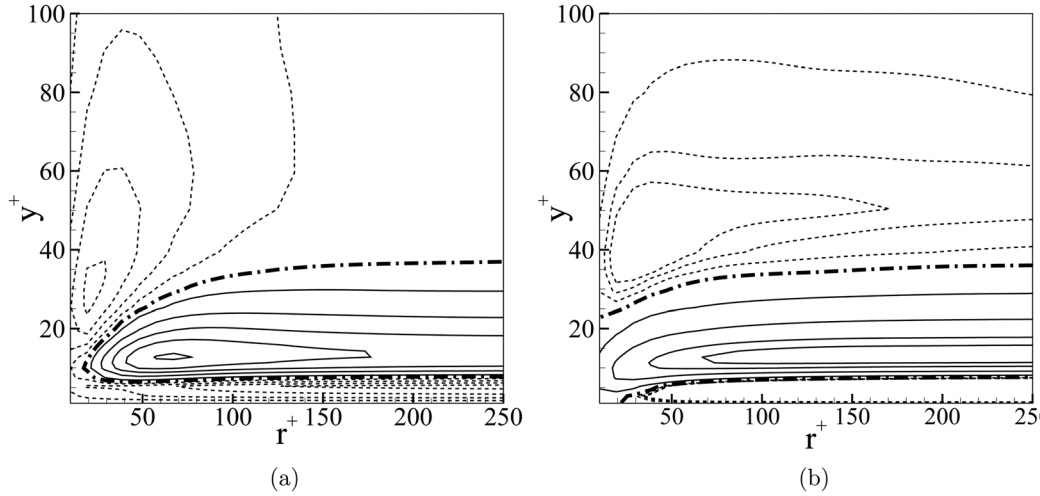

FIG. 5. (a) Contour plot of $T_r(r^+,y^+)$ (b) Contour plot of $T_c(r^+,y^+)$. In both plots, the zero contour line is shown by the dashed-dotted line. Positive contours are shown with solid lines and negative contours are shown with dashed lines. The data shown in these plots are from **Re590**.

Figures 5(a) and 5(b) show contours of T_r and T_c as a function of r^+ and y^+. In these figures, T_r and T_c are presented without the negative sign, which makes the convention different from the earlier scale energy plot in Figure 2. The zero crossing curve of T_r shown as the dashed-dotted line represents the location and scale where the switch between forward and reverse cascade occurs. In the viscous sublayer ($y^+ < 6$), T_r is always negative, implying that at all scales, a conventional energy cascade exists. In the region $6 < y^+ < 37$, the smallest scales still follow the direction of the conventional cascade, transferring energy to smaller and smaller eddies until it is dissipated by viscosity. At the larger scales, however, a net transfer of energy occurs from small to large scales. At $y^+ = 10$, this threshold of the change in transfer direction is $r^+ = 17$. At $y^+ = 30$, the threshold is at $r^+ = 72$. Beyond the buffer region at $y^+ > 37$, the normal cascade recovers for all scales.

In LES, backscatter refers to the energy being transferred from the modeled subgrid scales, to the larger computed grid scales. It is now widely accepted that it is necessary to incorporate backscatter into LES models to capture the flow physics accurately. The inverse cascade of energy observed in the current study is a clear manifestation of energy transfer from small to large scales. A number of studies have been conducted to understand and quantify the backscatter in turbulent channel flows by using filtered DNS data to mimic the effect of LES.[26–28] In particular, a study of a turbulent channel flow at $Re_\tau = 210$ pointed out that the subgrid scale transfer is a function of both the scale and the wall-normal location.[29] A contour plot of sub-grid scale transfer as a function of scale and distance from the channel wall was presented in that work. It was concluded that very close to the wall, the sub-grid scale transfer is positive, indicating a conventional transfer. Slightly further away from the wall, backscatter was observed for all scales. Beyond the region of backscatter, the conventional transfer was once again set up. These observations appear consistent with the results from the current study, although the present studies are extended to significantly higher Reynolds numbers including a more distinct logarithmic region.

T_c is plotted as a function of y^+ and r^+ in Figure 5(b). A positive value of T_c indicates a local removal of energy from that spatial location, while a negative value of T_c indicates a local supply of energy. Hence, this term reaches a maximum where the peak of scale energy occurs, which is within the buffer layer where the largest production of energy takes place. Similar to the trends observed in Figure 5(a), T_c is predominantly negative in the viscous sublayer. It can be observed that T_c is positive for $y^+ > 8$, which is smaller than the peak production location of $y^+ = 16$. At the lower edge of the logarithmic layer, T_c becomes negative once more, but with a very small magnitude, which does not play a significant part in the scale energy dynamics in the logarithmic layer. These observations conform to accepted notions of physical space energy transfer in wall-bounded turbulent flows.

E. Cross-over scale between production and scale transfer terms

The cross-over scale l_c^+ is the scale where the curves for $-\Pi_e$ and $-T_r$ intersect, as shown by the vertical dashed line in Figure 3(a). Thus, at scales smaller than l_c^+, the scale energy transfer is more significant, whereas at larger scales, the effective production becomes dominant. In Marati *et al.*, it was argued on the basis of dimensional arguments and classical equilibrium theory that l_c^+ is related to the shear scale $L_s = \sqrt{\langle\epsilon\rangle/S^3}$, where $S = dU/dy$.[2] In Figure 6(a), the filled triangles show the values of l_c^+ at **Re180**, which follow a linear trend for $20 < y^+ < 120$. The slope of this line was calculated as 0.37, approximately equal to the Karman constant κ. Thus, the value of the slope calculated at this small Reynolds number seemed physically reasonable. In fact, when the l_c^+ values from the higher Reynolds numbers are added to this plot, it is observed that they follow a very different trend and are consistently larger than those observed for **Re180**. Close to the wall ($y^+ < 50$), the values of cross-over scale from the three higher Reynolds number are very close to each other. For example, at $y^+ = 50$, the difference in cross-over scale between **Re300** and **Re934** is 3.5 wall units. However, beyond $y^+ = 50$, l_c^+ increases with increasing Reynolds number. A comparison of the trends of the curves in Figures 3(a) and 4(a) yields an explanation for this. Although the curves of $-\Pi_e$ do not change significantly with increasing Reynolds number, the transfer curves do. Higher T_r with Reynolds number results in larger values of l_c^+ at higher Reynolds numbers, hence the larger slopes at higher Reynolds numbers. Physically, this means that

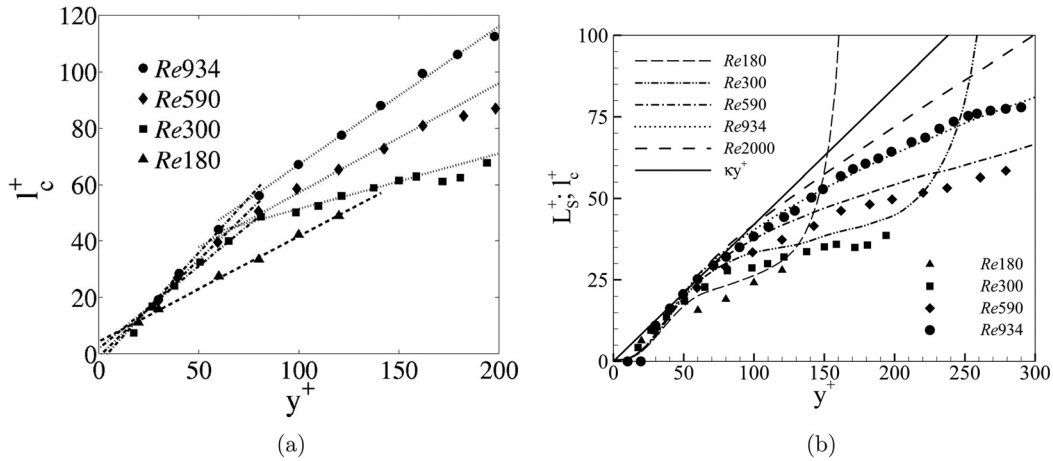

FIG. 6. (a) Variation of cross-over scale l_c^+ with y^+ for all DNS datasets. (b) Variation of shear scale L_s^+ and l_c^+ with y^+ for Reynolds numbers in the range $Re_\tau = 300$–2000. The straight line is the asymptotic prediction in the logarithmic layer κy^+. The symbols represent l_c^+ from the four Reynolds numbers rescaled by the same constant of order one chosen to match the shear scale for the largest available Reynolds number **Re934**.

beyond the buffer region, the range of transfer dominated scales increases with increasing Reynolds number. In order to better understand the trends observed, lines of best fit are also plotted in Figure 6(a). The presence of two distinct ranges and a change in slope in the range $60 < y^+ < 80$ is seen in all three higher Reynolds number cases. Close to the wall ($y^+ < 60$), the slopes of the best fit lines are 0.58 for **Re300**, 0.69 for **Re590**, and 0.78 for **Re934**. Further away from the wall ($60 < y^+ < 200$), the slopes of the lines decrease to 0.20 for **Re300**, 0.39 for **Re590**, and 0.49 for **Re934**. The difference is slope between the different Reynolds number increases with y^+, thus showing a fan-type behavior. At large y^+, each curve tends to asymptote to a constant value approaching the outer layer. The distinct presence of two ranges with linear variation of the cross over scale may have significant consequences. In fact, the linear increase of l_c^+ with y^+ that holds in the buffer-region, once better understood on physical grounds, in principle, could be exploited in large eddy simulations to understand the effect of the filter width, which close to the wall is typically in the production range above l_c^+.

Figure 6 shows the shear scale L_s^+ in the channel simulations for Reynolds numbers in the range $Re_\tau = 300$–2000.[30] In the figure, we added data at $Re_\tau = 2000$ to show the trend of the shear scale towards a well defined asymptotic behavior. The shear scale follows one linear trend close to the wall and a second one further away from the wall with a smaller slope, then goes to infinity at $y^+ = Re_\tau$. Upon increasing the Reynolds number, the shear scale recovers the asymptotic prediction in the logarithmic layer of κy^+, shown by the straight line. The symbols represent l_c^+ from the four Reynolds numbers we address in the scale energy analysis. Here, the l_c^+ values have been rescaled by the same constant of order one chosen to match the shear scale for the largest available Reynolds number **Re934**. At **Re934**, the rescaled l_c^+ matches the shear scale very well for the entire range of y^+ shown. The plots in Figure 6 thus reinforce the relationship between L_s^+ and l_c^+. Clearly, the dimensional estimate of the crossover scale as provided by the shear scale cannot take into account the presence of an order one dimensionless constant. Once the constant is extracted from the higher Reynolds number data, the two quantities collapse. Rescaling all the data with this value, the definite trend is that the two quantities, L_s^+ and the rescaled l_c^+, approach each other with increasing Reynolds number. We stress once more that below l_c^+, the Kolmogorov cascade should be asymptotically recovered. In conclusion, the cross-over scale is an ideal parameter to understand the dominant terms in the scale energy balance, and simultaneously provide a boundary between the isotropic and anisotropic scales in the flow.[18]

IV. SUMMARY AND CONCLUSIONS

The traditional method of classification of the momentum deficit region into the viscous sublayer, buffer region, logarithmic region, and outer region lacks information about the range of

scales and contributions of individual scales to the energy balance. Similarly, the spectral view of turbulence lacks spatial information about the physical distribution of eddies. The methodology presented here combines these complementary approaches to provide a unified technique of analyzing wall-bounded turbulent flows. It was previously utilized with Direct Numerical Simulation (DNS) data of a channel flow at a friction Reynolds number of $Re_\tau = 180$ where significant low Reynolds number effects emerged.[2] This paper extends the analysis to higher Reynolds numbers in the range $Re_\tau = 300$–934 to document the effects of increasing Reynolds number.

Comparing the results of the scale energy analysis for **Re300**, **Re590**, and **Re934**, the viscous sublayer and buffer regions were found to have reached a Reynolds independent state as shown by the matching of the different terms of the budget across the entire range of available scales. Further away from the wall in the logarithmic region, the transfer of energy across scales increased with Reynolds number, while the production of energy remains constant with increasing Reynolds number. In order to balance the increased transfer of energy, the dissipation of turbulent kinetic energy increased with Reynolds number. As previously observed at $Re_\tau = 180$, the present data confirm the existence of a range of scales in the buffer layer where energy flows from the smaller to the larger scales, indicating a reverse energy cascade associated with the near-wall turbulent kinetic energy production cycle. The spatial flux departs from this region, indicating a net transfer of energy both towards the wall and the bulk of the flow. In the present study, this envelope has been characterized for **Re590** and **Re934**, and this envelope is observed in the range $6 < y^+ < 37$, where all scales except the smallest scales display characteristics of an inverse energy cascade. Though a proper logarithmic region may not be fully formed at the present Reynolds numbers, a region crossed by a substantially constant energy flux towards the outer region is nevertheless clearly observed at the higher Reynolds number. Here the energy transfer among scales goes systematically from large to small, recovering the classical Richardson view of the turbulent cascade. In this region, the strength of the cascade and the production of scale energy increases with Reynolds number.

One of the interesting aspects of the present approach is its capability to assess the distribution of energy production and energy transfer in a spectrum of scales as a function of the distance from the wall. Specifically, two ranges are identified, dominated by energy production and energy transfer, respectively. The cross-over scale between these two ranges is found to increase linearly with distance from the wall up to the lower logarithmic region, with its slope relatively independent of the Reynolds number. The slope of this curve is distinctly larger than that found previously using the **Re180** data. Further away from the wall, the cross-over scale still grows linearly; however, the slope increases with increasing Reynolds number. The difference in cross-over scale with Reynolds number is amplified at higher y^+, such that these lines exhibit a fan-type behavior. The transition between the two types of linear behaviors occurred at around $y^+ = 60$ for the three higher Reynolds number datasets. Also, a direct relation between l_c^+ and the dimensional estimate of the shear scale is confirmed by the present data, such that the shear scale could be used to predict the crossover scale. These results involving production and transfer dominated scales may find application in the context of large eddy simulations, where a clear understanding of the dominant dynamics within the filtered range of scales may be helpful for improved numerical modeling of the wall region.

ACKNOWLEDGMENTS

The authors wish to acknowledge Professor Robert Moser for providing the two higher Reynolds number DNS datasets and Dr. Nicoletta Marati for the initial development of the scale energy analysis. I.M. wishes to acknowledge the support of the Australian Research Council. This work was supported by the National Science Foundation through Grant No. CTS-0324898.

[1]R. J. Hill, "Exact second-order structure-function relationships," J. Fluid Mech. **468**, 317 (2002).
[2]N. Marati, C. M. Casciola, and R. Piva, "Energy cascade and spatial fluxes in wall turbulence," J. Fluid Mech. **521**, 191 (2004).
[3]T. Wei, P. Fife, J. Klewicki, and P. McMurtry, "Properties of the mean momentum balance in turbulent boundary layer, pipe and channel flows," J. Fluid Mech. **522**, 303 (2005).
[4]P. Fife, T. Wei, J. Klewicki, and P. McMurtry, "Stress gradient balance layers and scale hierarchies in wall-bounded turbulent flows," J. Fluid Mech. **532**, 165 (2005).

[5]T. Wei and W. W. Willmarth, "Reynolds-number effects on the structure of a turbulent channel flow," J. Fluid Mech. **204**, 57 (1989).
[6]D. B. De Graaff and J. K. Eaton, "Reynolds number scaling of the flat-plate turbulent boundary layer," J. Fluid Mech. **422**, 319 (2000).
[7]R. A. Antonia, M. Teitel, J. Kim, and L. W. B. Browne, "Low-Reynolds-number effects in a fully developed turbulent channel flow," J. Fluid Mech. **236**, 579 (1992).
[8]R. D. Moser, J. Kim, and N. N. Mansour, "Direct numerical simulation of turbulent channel flow up to $Re_\tau = 590$," Phys. Fluids **11**, 943 (1999).
[9]H. Abe, H. Kawamura, and Y. Matsuo, "Direct numerical simulation of a fully developed turbulent channel flow with respect to the Reynolds number dependence," J. Fluid Eng. **123**, 1755 (2001).
[10]S. Hoyas and J. Jiménez, "Reynolds number effects on the Reynolds-stress budgets in turbulent channels," Phys. Fluids **20**, 101511 (2008).
[11]P. Bradshaw, "Inactive motion and pressure fluctuations in turbulent boundary layers," J. Fluid Mech. **30**, 241 (1967).
[12]J. Kim, P. Moin, and R. D. Moser, "Turbulence statistics in fully developed channel flow at low Reynolds number," J. Fluid Mech. **177**, 133 (1987).
[13]A. Cimarelli and E. De Angelis, "Analysis of the Kolmogorov equation for filtered wall-turbulent flows," J. Fluid Mech. **676**, 376 (2011).
[14]J. C. del Álamo, J. Jiménez, P. Zandonade, and R. D. Moser, "Scaling of the energy spectra of turbulent channels," J. Fluid Mech. **500**, 135 (2004).
[15]P. A. Davidson, *Turbulence: An Introduction for Scientists and Engineers* (Oxford University Press, New York, 2004).
[16]S. B. Pope, *Turbulent Flows* (Cambridge University Press, Cambridge, England, 2000).
[17]M. Fischer, J. Jovanović, and F. Durst, "Reynolds number effects in the near-wall region of turbulent channel flows," Phys. Fluids **13**, 1755 (2001).
[18]B. Jacob, C. M. Casciola, A. Talamelli, and P. H. Alfredsson, "Scaling of mixed structure functions in turbulent boundary layers," Phys. Fluids **20**, 045101 (2008).
[19]J. L. Lumley, "Interpretation of time spectra measured in high-intensity shear flows," Phys. Fluids **8**, 1056 (1965).
[20]N. Hutchins and I. Marusic, "Large-scale influences in near-wall turbulence," Proc. R. Soc. Lond. A **365**, 647 (2007).
[21]N. Hutchins and I. Marusic, "Evidence of very long meandering features in the logarithmic region of turbulent boundary layers," J. Fluid Mech. **579**, 1 (2007).
[22]S. Hoyas and J. Jiménez, "Scaling of the velocity fluctuations in turbulent channels up to $\mathrm{Re}_\tau = 2003$," Phys. Fluids **18**, 011702 (2006).
[23]R. Mathis, N. Hutchins, and I. Marusic, "Large-scale amplitude modulation of the small-scale structures in turbulent boundary layers," J. Fluid Mech. **628**, 311 (2009).
[24]S. J. Kline, W. C. Reynolds, F. A. Schraub, and P. W. Runstadler, "The structure of turbulent boundary layers," J. Fluid Mech. **30**, 741 (1967).
[25]C. M. Casciola, P. Gualtieri, R. Benzi, and R. Piva, "Scale-by-scale budget and similarity laws for shear turbulence," J. Fluid Mech. **476**, 105 (2003).
[26]U. Piomelli, W. H. Cabot, P. Moin, and S. Lee, "Subgrid-scale backscatter in turbulent and transitional flows," Phys. Fluids **3**, 1766 (1991).
[27]C. Härtel, L. Kleiser, F. Unger, and R. Friedrich, "Subgrid-scale energy transfer in the near-wall region of turbulent flows," Phys. Fluids **6**, 3130 (1994).
[28]U. Piomelli, Y. Yu, and R. J. Adrian, "Subgrid-scale energy transfer and near-wall turbulence structure," Phys. Fluids **8**, 215 (1996).
[29]J. A. Domaradzki, W. Liu, C. Härtel, and L. Kleiser, "Energy transfer in numerically simulated wall-bounded turbulent flows," Phys. Fluids **6**, 1583 (1994).
[30]The statistics for **Re2000** are available at http://torroja.dmt.upm.es/ftp/channels/data/.